Journal of Applied Electrochemistry **30**: 411–418, 2000.

Durability test of SOFC cathodes

M.J. JØRGENSEN, P. HOLTAPPELS and C.C. APPEL*
Materials Research Department, Risø National Laboratory, PO Box 49, DK-4000 Roskilde, Denmark
**Present address: Geological Survey of Denmark and Greenland, Thoravej 8, DK-2400 Copenhagen NV, Denmark*

Received 25 May 1999; accepted in revised form 21 September 1999

Key words: cathodes, degradation, durability, lanthanum strontium manganite, solid oxide fuel cell, structure

Abstract

The durability of solid oxide fuel cell (SOFC) composite cathodes of lanthanum strontium manganite and yttria stabilised zirconia was investigated. The cathodes were kept at constant, realistic operating conditions (−300 mA cm^{-2} at 1000 °C in air) for up to 2000 h. After the 2000 h test the increase in electrode overvoltage exceeded 100% of the initial value. Nominally identical cathodes kept for 2000 h at 1000 °C in air without current load for comparison showed little or no degradation. Thus, the current load of −300 mA cm^{-2}, rather than the operation temperature of 1000 °C, was responsible for the degradation. Structural analysis showed an increase in the porosity at the electrode interfaces, when the electrode had been polarised. No such structural changes were found for electrodes tested without current load. The degradation is primarily ascribed to pore formation in the electrode material induced by an electric field.

1. Introduction

Solid oxide fuel cells are one of the most promising future power generation technologies. An important issue with respect to reduction of the cost per unit of electricity produced by an SOFC stack is the durability of the cell. It is useful to study the ageing of the individual cell components in order to gain a better understanding of the fundamentals behind the degradation of SOFCs. In the present work the cathode is investigated.

The classical SOFC cathode material is strontium doped lanthanum manganite (LSM) [1]. It is advantageous to produce the cathode as a composite of LSM and the electrolyte material, zirconia stabilised by yttria (YSZ) [2,3]. Thereby, the electrochemically active reaction zone may be extended from the interface between the electrode and the electrolyte to the bulk of the electrode.

The performance of composite cathodes depends on the microstructure [4–7]. Therefore, microstructural changes during operation may change the performance considerably. Furthermore, the performance may depend on the formation of low-conductive reaction products such as lanthanum zirconate at the cathode–electrolyte interface during cell fabrication. An A-site deficient LSM composition was used for the cathodes in the present work, as this composition minimises the formation of lanthanum zirconate during fabrication [8].

To increase the understanding of the degradation of SOFC composite cathodes it is relevant to investigate whether temperature, current load or kinetic processes are responsible for the degradation. In the present work the degradation of SOFC cathodes operated at realistic conditions for up to 2000 h was studied. Nominally identical cathodes, which were annealed at high temperature, but not exposed to current during the annealing period, were studied for comparison. The aim was to separate the effect of temperature and current on the degradation of the cathodes.

The study combines electrochemical methods with scanning electron microscopy (SEM) and energy dispersive X-ray spectrometry (EDS). Changes in electrochemical performance are compared with the changes in microstructure and composition of the cathode and the electrolyte.

2. Experimental details

2.1. *Sample preparation*

Electrolyte substrates were produced from YSZ with 8 mol % Y_2O_3 (TZ8Y, Tosoh Corporation, Japan). Pellets were pressed, machined to the shape shown in Figure 1 and then sintered at 1600 °C. The area of the working electrode was approx. 0.4 cm^2.

Two types of electrodes were tested; type A comprising a composite electrode layer (denoted C-layer), and type B comprising a C-layer and a current collecting layer (denoted CCC-layer).

The C-layer was made from a mixture of 60 wt % LSM and 40 wt % YSZ. The LSM material

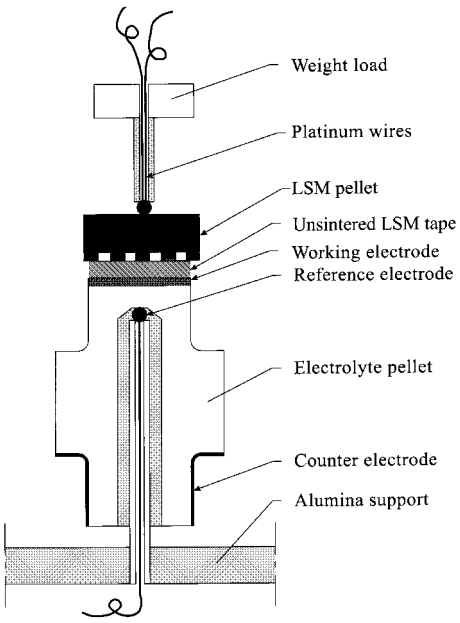

Fig. 1. Schematic of the electrochemical three-electrode, four-wire setup.

$(La_{0.85}Sr_{0.15})_{0.9}MnO_{3\pm\delta}$ (nominal composition, Haldor Topsøe A/S, Denmark) was produced by spray pyrolysis using organic complex combustion synthesis [9]. The YSZ fraction of the C-layer contained 3 mol % Y_2O_3 (TZ–3YB, Tosoh Corporation, Japan).

The C-layer was made by airborne spray coating a low-viscous slurry on the electrolyte substrate. The spray coat slurry was produced by ball milling the powders with dispersant and ethanol. The C-layer was sintered at 1300 °C for 2 h. After sintering the thickness of the C-layer was 5–20 μm.

On electrodes of type B a CCC-layer consisting of two layers of pure LSM aimed for current collection were applied on the sintered C-layer by spray coating. The layers were sintered individually at 1300 °C for 2 h. The total thickness of the two layers was 15–30 μm after sintering.

On electrodes of both type A and B an unsintered tape cast LSM foil for current collection was applied on the working electrode immediately before the electrochemical test. The LSM foil was approximately 40 μm thick after binder burnout during approach to test temperature. A dense, channelled LSM pellet was pressed into contact with the LSM foil (Figure 1) to ensure optimum current pick-up from the working electrode during the test.

The construction and electrochemical treatment of the electrodes are shown in Table 1 together with an ID code for each type of treatment. In the following the ID codes A or B have the subscript 'galv' (for instance, A_{galv}), when galvanostatic durability test was performed, whereas no subscript is used for the electrodes in the nonloaded durability test. The subscript 'ref.' is used for reference samples, which were produced in parallel with the other samples and were used only for structural analysis.

2.2. *Electrochemical test*

The composite electrodes were tested electrochemically using the three-electrode, four-wire set-up shown in Figure 1. The counter electrode consisted of Pt paste, while the reference electrode was a Pt bead. Four electrochemical cells were placed in a furnace and measurements were performed on one cell at a time. The test atmosphere was air.

The test procedure used for the different types of electrodes is shown in the flow chart in Figure 2. The durability tests were performed as follows. Impedance measurements at open circuit voltage (OCV) and under four fixed cathodic polarisations were performed at 850, 950 and 1000 °C in air before and after the durability test. The impedance measurements were performed after an equilibration period of 15 min at each potential. Durability test at 1000 °C in air was performed with or without a galvanostatic load of -300 mA cm^{-2} in up to 2000 h.

The measurements were carried out using different combinations of instruments from Solartron (S1260 + S1287, S1250 + S1286 or S1280). The maximum frequency used in the impedance measurements varied with the used frequency response analyser (20–65 kHz). The lowest measuring frequency was 5 mHz for the first OCV measurement and 50 mHz for all other impedance measurements. The amplitude applied between the working and the reference electrode was 14 mV (r.m.s.) and six points per decade were measured.

During the galvanostatic durability test a constant current of -300 mA cm^{-2} was applied between the working and the counter electrode. The voltage drop at each cathode was measured between the reference electrode and a potential probe connected to the working electrode

Table 1. Description of the electrodes tested

ID	Construction	Durability test	Aim
A	C + tape	0 mA cm^{-2}	Determine effect of temperature. Compare with $A_{ref.}$, A_{galv} and B.
A_{galv}	C + tape	-300 mA cm^{-2}	Determine effect of temperature and current. Compare with $A_{ref.}$, A and B_{galv}.
$A_{ref.}$	C + tape	No test	Reference used for structural analysis. Not tested electrochemically.
B	C + CCC + tape	0 mA cm^{-2}	Determine effect of temperature. Compare with A and $B_{ref.}$, B_{galv}.
B_{galv}	C + CCC + tape	-300 mA cm^{-2}	Determine effect of temperature and current. Compare with A_{galv} and $B_{ref.}$, B.
$B_{ref.}$	C + CCC + tape	No test	Reference used for structural analysis. Not tested electrochemically.

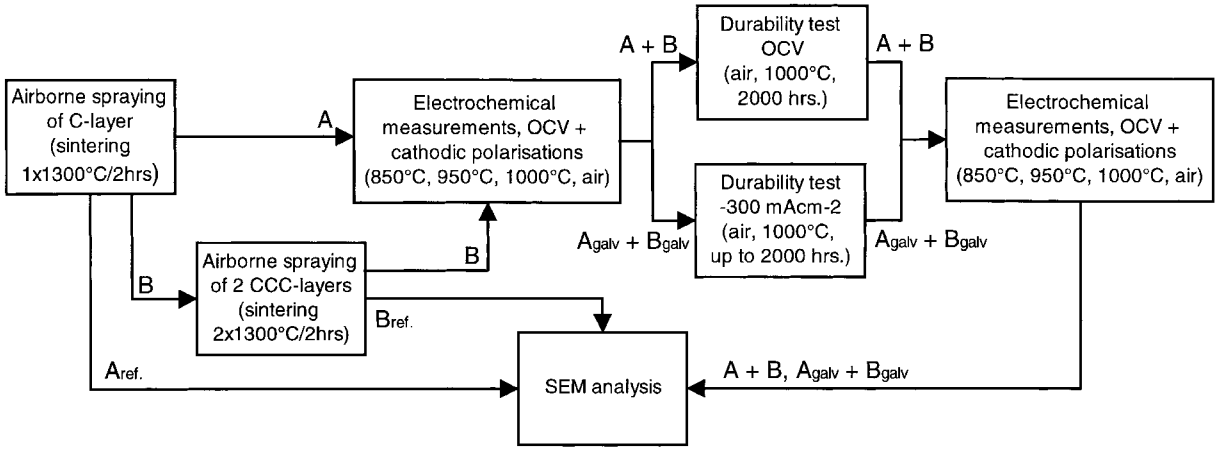

Fig. 2. Flow chart showing the sample preparation and test. Electrode type (A or B) is marked in the flow chart.

(four-wire, three-electrode setup). Impedance measurements were performed approximately every 200 h at the actual measured potential. The current was supplied by a Danica TPS 20 constant current supply. The voltage difference between the working and the reference electrode was measured by a Fluke multimeter.

The unloaded durability tests were performed by placing the samples in a separate furnace for two periods of 1000 h. The electrode performance was measured before and after each heat treatment (Figure 2).

2.3. *SEM investigations*

Electrodes for structural analysis were embedded in epoxy by a vacuum technique to preserve the structure during the further sample preparation. The samples were cut perpendicular to the cathode–electrolyte interface, ground and polished. The samples were examined by scanning electron microscopy (SEM) (Jeol LV5310). X-ray element mapping was performed on a Philips XL40 SEM with a Noran Vantage EDS system.

3. Results

3.1. *Durability test*

Current–overvoltage curves measured at 1000 °C for electrodes of type A and B before and after durability test are shown in Figure 3(a) and (b), respectively. The ohmic resistance, R_s, which was used for correction for the ohmic drop of the electrolyte substrate, was obtained from impedance data using the EQUIVCRT program [10]. The current–overvoltage curves are assumed to be linear at low overvoltages, that is, the slope of the curve corresponds to the inverse d.c. resistance.

According to Figure 3(a) almost no degradation was found after the unloaded durability test (type A), while the electrodes degraded considerably during the galvanostatic durability test (type A_{galv}). Similar results were obtained for electrodes of type B and B_{galv}, respectively (Figure 3(b)). The same difference between the degradation of the electrodes in the galvanostatic and the unloaded test, respectively, was found at 850 °C.

Figure 4 shows the change in overvoltage with time for electrodes of type A_{galv} and B_{galv} during the galvanostatic durability test. For three of the electrodes the degradation rate was smaller during the first 800 h compared to the last 1000 h (concave overvoltage-time curve). For the fourth electrode the degradation rate was constant within the tested period (linear overvoltage-time curve). After 2000 h galvanostatic durability test the increase in overvoltage at 1000 °C exceeded 100% of the initial value for all the electrodes. The increase in overvoltage with time was most severe for electrodes without sintered CCC-layer (type A_{galv}) compared with electrodes with this layer (type B_{galv}).

Examples of the time dependence of the ohmic resistance R_s, which was mainly ascribed to the electrolyte, are also plotted in Figure 4. The increase in R_s with time was comparable with the degradation rate, that is, increase in resistivity, measured for YSZ (with 8 mol % Y_2O_3) slightly doped with Mn [11].

Impedance spectra measured at OCV before and after galvanostatic durability test on an electrode of type A_{galv} are shown in Figure 5. The initial impedance (Figure 5(a)) applied well to the model presented by Holtappels et al. [12]. After the durability test the impedance was changed considerably at both high and low frequencies.

3.2. *SEM investigations*

Six types of electrodes were investigated using SEM. Reference samples ($A_{ref.}$ and $B_{ref.}$), electrodes subjected to non-loaded durability test (A and B), and electrodes tested galvanostatically (A_{galv} and B_{galv}). A number of micrographs taken systematically along the electrode–electrolyte interface were studied for each type of electrode. Along this interface for one particular electrode considerable variations in the microstructure and pore size distribution were found. Also variations in the

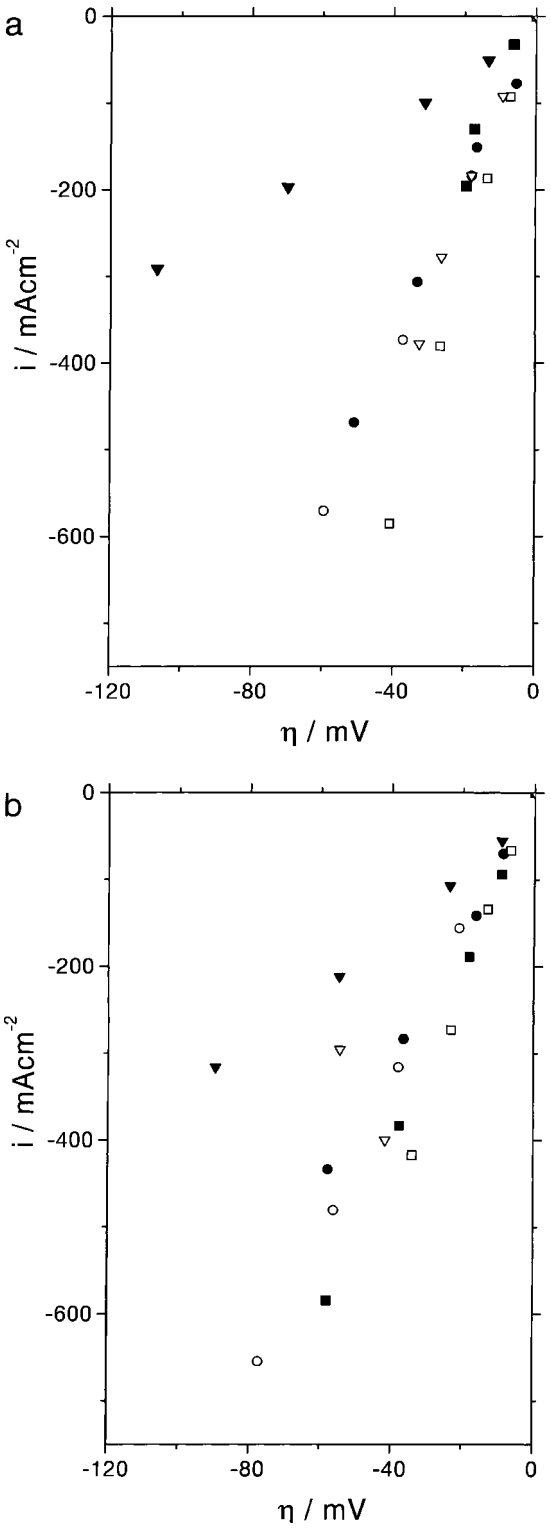

Fig. 3. Steady state current against overvoltage curves. Measurement conditions: 1000 °C, air. (a) Type A: (○) before test, (□) after 1000 h, (▽) after 2000 h. Type A_{galv}: (●) sample 1, before test, (■) sample 2, after 1000 h, (▼) sample 3, after 2000 h. (b) Type B: (○) before test, (□) after 1000 h, (▽) after 2000 h. Type B_{galv} (●) sample 1, before test, (■) sample 1, after 1000 h, (▼) sample 2, after 2000 h.

thickness of the C-layer and CCC-layer across the interface were found. Due to these variations for each sample the microstructural results presented in the following only include trends where significant micro-

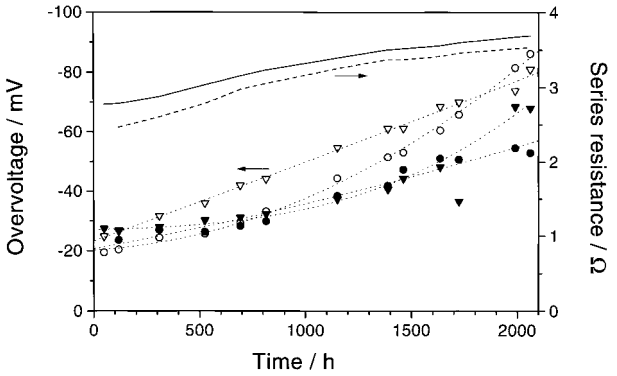

Fig. 4. Overpotential and series resistance against time obtained in durability tests at 1000 °C in air. Overvoltage: (○,▽) A_{galv}, (●,▼) B_{galv}. Series resistance: solid line: A_{galv}, dashed line: B_{galv}.

structural changes were observed after the durability test.

Micrographs with the same magnification of electrodes of type $A_{ref.}$, A, A_{galv} and $B_{ref.}$, B, B_{galv} are shown in Figures 6 and 7, respectively. The micrographs of the reference electrodes in Figures 6(a) and 7(a) show that the C-layers in general had very dense areas with a random distribution of 3–10 μm pores. The adhesion between the C-layer and the electrolyte was good. No obvious change in the C-layer microstructure seemed to occur during the nonloaded durability test. The microstructure of type A might seem more open after the nonloaded durability test (compare Figures 6(a) and (b)). This is considered to be within the expected structural variation of the C-layer.

For the electrodes tested galvanostatically (type A_{galv} and B_{galv}) changes in the microstructure at the C-layer interfaces were found. This is illustrated in Figures 6(c) and 7(c) and 7(d), where small pores ($\sim$1 μm) along the interfaces of the C-layer are visible. These pores were neither found in the reference electrodes (Figures 6(a) and 7(a)), nor in the electrodes tested without current load (Figures 6(b) and 7(b)).

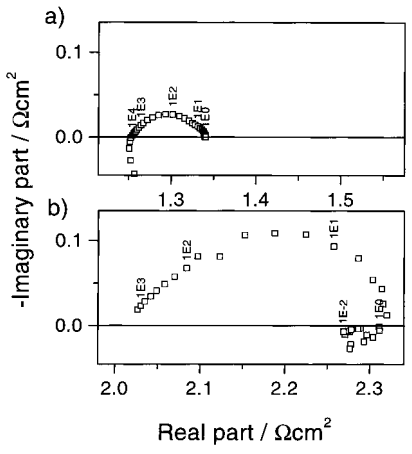

Fig. 5. Impedance spectra taken at open circuit voltage (a) before and (b) after current loaded durability test (−300 mA cm^{-2} for 2000 h) for an electrode without CCC-layer (type A_{galv}). Measurement conditions: 1000 °C, air.

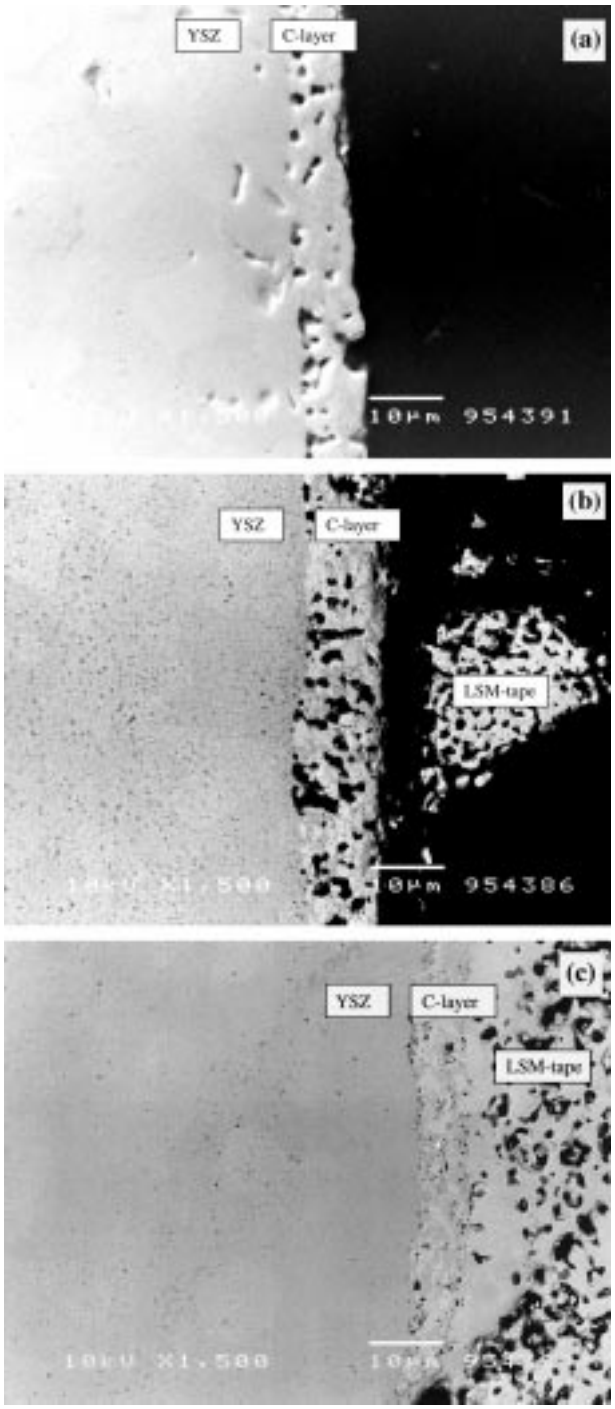

Fig. 6. Back-scattered electron images of electrodes without CCC-layers (type A) tested in air at 1000 °C. (a) reference sample (type $A_{ref.}$), (b) after 2000 h without current load (type A), (c) after 2000 h with current load (type A_{galv}).

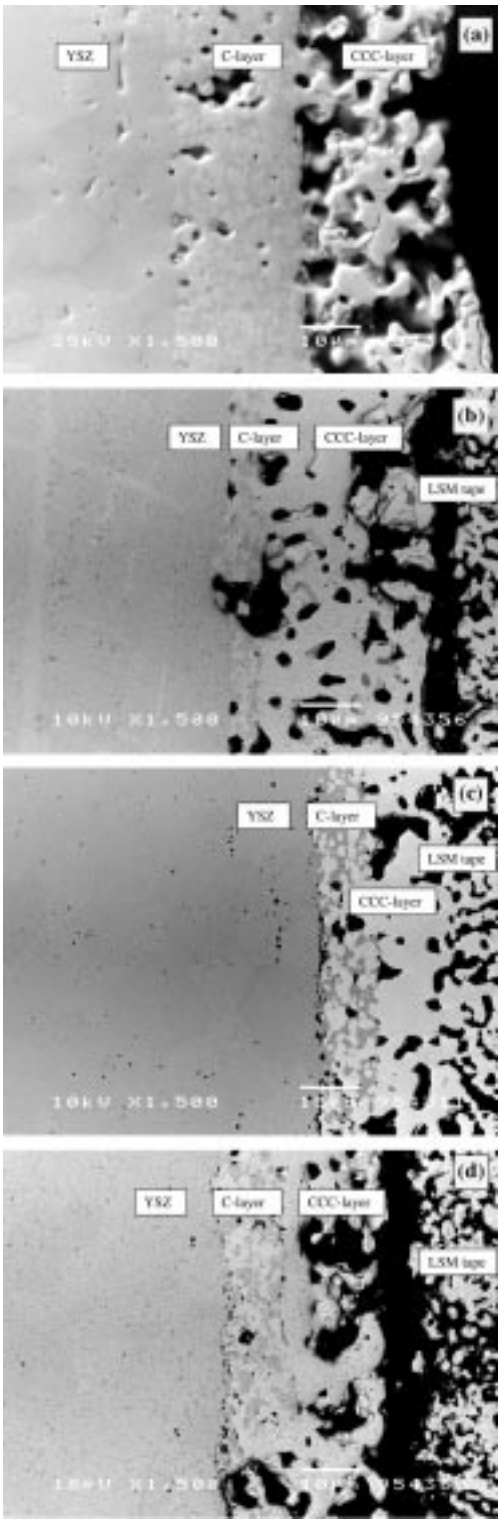

Fig. 7. Backscattered electron images of electrodes with CCC-layers (type B) tested in air at 1000 °C. (a) Reference sample (type $B_{ref.}$), (b) after 2000 h without current load (type B), (c) after 1000 h with current load (type B_{galv}), (d) after 2000 h with current load (type B_{galv}).

For electrodes with only a C-layer (type A_{galv}) the C-layer and the current collecting LSM-tape closest to the C-layer interface had densified during the galvanostatic test (cf. Figure 6(a) and (c)). For electrodes including CCC-layer (type B_{galv}) the possible densification of the C-layer after 2000 h galvanostatic durability test (Figure 7(d)) was not as pronounced as for type A_{galv}.

X-ray element mappings at the interface between the C-layer and the electrolyte were made for electrodes of type B and B_{galv}. In both cases the Mn concentration was found to be higher along the grain boundaries of the electrolyte material close the interface than inside the electrolyte grains (Figure 8). No difference in the Mn concentration at the grain boundaries was found for

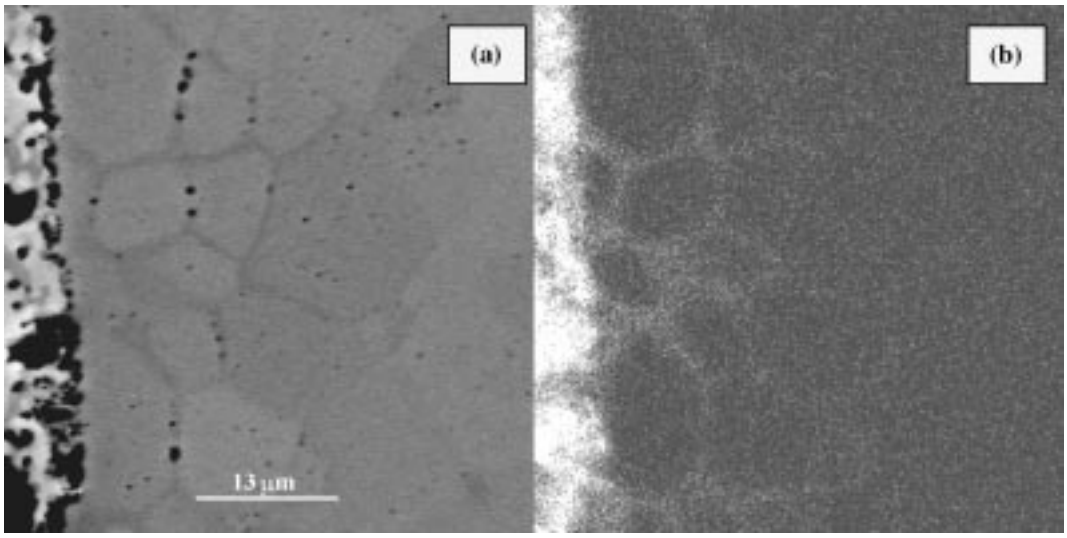

Fig. 8. (a) Backscattered electron image of a cathode–electrolyte interface type B_{galv}. Grain boundaries in YSZ close to interface are dark. (b) X-ray map of MnK_α. A higher concentration of Mn in the grain boundaries than in grains of YSZ is observed.

electrodes tested with and without current load (type B and B_{galv}).

Variations in the relative concentration of the elements in the C-layer-electrolyte interface were examined by EDS point analyses. This did not show formation of reaction products such as La-zirconate. The white particles seen in the C-layer in Figure 6(c) were found to consist of Pt. Deposition of Pt in the electrode structure during operation is not likely, as there is no Pt in the vicinity of the electrode during the experiments. Therefore, Pt is assumed to be a contamination from the cutting and polishing process.

4. Discussion

The results of the unloaded durability tests (type A and B) showed that keeping the electrodes at OCV and 1000 °C for 2000 h did not cause considerable degradation. However, when current was passed through the electrodes at otherwise identical conditions the degradation was severe. Therefore, the current load of -300 mA cm^{-2} rather than the operation temperature of 1000 °C was responsible for the degradation.

In the following emphasis will be put on the microstructural changes observed by SEM after galvanostatic durability test. The results did not indicate formation of reaction products such as La-zirconate or enhanced migration of cations from the C-layer to the electrolyte for galvanostatically tested electrodes. Therefore, the degradation is not considered to be related to these phenomena, and they will not be discussed further.

4.1. *Microstructural changes*

Two types of microstructural changes were observed for galvanostatically tested electrodes, pore formation at the C-layer interfaces and densification of the C-layer and the current collecting tape on electrodes of type A_{galv}. These two phenomena will be treated separately in the following.

The observed pore formation at the C-layer interfaces might have caused a decrease in the length of active triple phase boundary (TPB) between electrode, electrolyte and gas phase, as the contact area between C-layer and electrolyte was decreased considerably (for instance, see Figure 7(c)). As the polarisation resistance scales with the inverse of TPB length, the microstructural changes might be responsible for the observed increase in polarisation resistance during galvanostatic tests.

In electrodes of type A_{galv} densification of the C-layer during galvanostatic durability test (compare Figures 6(a) and (c)) may have decreased the length of the TPB further, causing these electrodes to degrade more than electrodes of type B_{galv} (Figure 4). The densification was presumably related to sintering of the structure due to ohmic heating. Electrodes of type A_{galv} were more likely to sinter during the test, as they were only sintered once at 1300 °C, while electrodes of type B_{galv} were sintered three times at these conditions (Figure 2).

The densification of the current collecting LSM-tape on electrodes of type A_{galv} during galvanostatic test (cf. Figures 6(a) and (c)) is presumably due to sintering of the tape-structure during current load, as this layer was unsintered at the beginning of the test. This densification may also decrease the electrode performance, as the interface between the C-layer and the current collecting layer has previously been found to affect the electrode performance [7].

The pore formation observed after the galvanostatic durability test was a common feature for all the cathodes investigated. Since closed pores may contribute as extra capacitive contributions in the electrode impedance [13], the appearance of an extra capacitive arc at high frequencies in Figure 5(b) is not contradictory to the assumption that mainly the pore formation affected

the degradation of the electrochemical performance. In the following this feature is discussed in more detail.

Pore formation between LSM and YSZ induced by current load has also been found by Tsukuda and Yamashita [14]. They observed voids at the interface between LSM and YSZ grains in some samples after 18.5 h test at 0.5 A cm^{-2} at 1000 °C. An increase in polarization resistance due to the voids was not measured, on the contrary the performance improved. The reason for this might be that the pore formation was much less extensive than in the present work, probably due to the short test period.

Other authors have found microstructural changes at the interface between an electrode and a YSZ electrolyte after current load. Bay and Jacobsen [15,16] found that the morphology of the interface between a Pt point electrode and a YSZ electrolyte changed during a potentiostatic experiments at 1000 °C. The changes were related to passage of current, as the material at the YSZ surface did not redistribute after annealing at 1000 °C without current load [16]. No explanations about possible driving forces for this severe mass transport were given.

Mass transport by so called 'kinetic demixing' of multicompound ceramic oxide materials due to electrotransport has been described in literature [17–20]. When such materials are exposed to an electric field local thermodynamic equilibrium does not exist, causing the materials composition to change locally [17]. Hong and Yoo [19] found that differences in both diffusivity and effective charge of the cations in a multi-compound ceramic oxide are responsible for the redistribution of the elements. Yoo and Lee [20] warned that kinetic demixing could be relevant for SOFC materials such as YSZ and LSM.

When exposing a cation deficient oxide material to an oxygen potential gradient cations can migrate towards the higher oxygen potential interface, while vacancies move in the opposite direction. This may lead to pore formation and pore movement [17]. The pores will preferably form at the interface with the lowest oxygen potential in places, where there is an indentation or a notch, as this part of the interface is unstable. The pores are transported towards the interface with the highest oxygen potential. This prediction seems also to be fullfilled in our studies where the pores are presumably formed at the C-layer-electrolyte interface (low-potential interface) and transported towards the CCC-layer (see for instance Figure 6(c)). The applied current creates an oxygen potential difference across the C-layer and this difference may be the driving force of the pore formation.

From the above discussed results we conclude that, among other factors, for example, sintering properties of the cathode layers, the thermodynamic stability of the multicomponent ceramic mixture under operating conditions turns out to be an important factor determining the long time performance of SOFC cathodes. However, the SEM resolution is too low to prove that redistribution of the cathode components occurs during galvanostatic test, and measurement techniques with higher resolution should be used to confirm this. The composite nature of the cathode complicates matters, as the YSZ phase in the electrode may affect the expected demixing.

4.2. *Impact on fuel cell operation*

The above mentioned theory about electrotransport phenomena suggests that the magnitude of the current load will affect the pore formation rate. This is confirmed by a comparison of the results obtained in the present work with literature results [21]. Cells comprising cathodes produced with the same materials compositions and manufacturing procedures as the cathodes in the present work have been tested for 2000 h in a stack [21]. During the first 1100 h the stack was operated at approximately 0.13 A cm^{-2}, after that the current load was varying. The degradation of the electrodes was considerably lower than what could be expected from the results reported above. For some cells essentially no degradation was found after 2000 h of operation. No voids at the C-layer interfaces were found after the test [22]. The reason for this is presumably that the stack was operated at a smaller current load/overvoltage than the electrodes tested in the present work.

The thermodynamic stability of LSM–YSZ composite cathodes may vary with parameters such as materials compositions and microstructure. Furthermore, the operating conditions (current load/overvoltage) may affect the long time performance, as illustrated by the results presented above. In order to secure a long lifetime for SOFC cathodes, it is crucial to explore the cause of the deterioration further and to find precautions against it. It is relevant to search for electrode compositions and microstructures which are stable when exposed to a potential difference across the material.

5. Conclusions

Composite LSM/YSZ electrodes tested without current load showed little or no degradation after 2000 h at 1000 °C in air. For electrodes tested galvanostatically at −300 mA cm^{-2} and 1000 °C in air an increase in overvoltage exceeding 100% of the initial value was found after 2000 h test.

A characterization of the electrodes by SEM showed that a large number of less than 1 μm pores were formed close to the interfaces of the composite cathode layer for electrodes tested galvanostatically. No such structural changes were observed after the unloaded durability tests.

For electrodes without a sintered current collecting layer a densification of the composite layer and the LSM-tape aimed for current collection occured during galvanostatic test.

The morphology change due to pore formation and densification of the composite layer for electrodes without a sintered current collecting layer are assumed

to be the main reasons for the increase in the polarization resistance during the galvanostatic durability test, due to a decrease in the active triple phase boundary length.

The current load presumably created an oxygen potential difference across the composite cathodes. This may have lead to the observed pore formation and pore movement. Electrotransport of components in the LSM may lead to redistribution of the cathode material. The mechanisms of the structural changes needs further examination, in order to identify possible precautions against deterioration of the LSM cathodes.

Acknowledgement

This work was performed as part of the European project 'Improved Durability of SOFC Stacks', Contract no. JOE3-CT95-0005. Colleagues at Risø National Laboratory are kindly acknowledged for the supply of samples and fruitful discussions. Special thanks to Dr. P.V. Hendriksen, Risø Nat. Lab. for inspiring discussions. C.C. Appel publishes with the permission of the Geological Survey of Denmark and Greenland.

References

1. N.Q. Minh and T. Takahashi, 'Science and Technology of Ceramic Fuel Cells' (Elsevier Science BV, 1995), p. 118.
2. T. Kenjo and M. Nishiya, *Solid State Ionics* **57** (1992) 295.
3. M.J.L. Østergård, C. Clausen, C. Bagger and M. Mogensen, *Electrochim. Acta* **40** (1995) 1971.
4. J. Mizusaki, H. Tagawa, K. Tsuneyoshi and A. Sawata, *J. Electrochem. Soc.* **138** (1991) 1867.
5. F.H. van Heuveln, F.P.F. van Berkel and J.P.P. Huijsmans, *in* Proc. 14th Risø International Symposium on 'Material Science', Denmark, edited by F.W. Poulsen, J.J. Bentzen, T. Jacobsen, E. Skou and M.J.L. Østergård (1993), p. 53.
6. K. Sasaki, J.P. Wurth, M. Gödickemeier, A. Mitterdorfer and L.J. Gauckler, in Proc. 4th International Symposium on 'SOFC', Japan, edited by M. Dokiya, O. Yamamoto, H. Tagawa and S.C. Singhal (1995), p. 625.
7. M. Juhl, C. Manon, S. Primdahl, M. Mogensen, *J. Power Sources* **61** (1996) 173.
8. C. Clausen, C. Bagger, J.B. Bilde-Sørensen, A. Horsewell, *Solid State Ionics* **70**/**71** (1994) 59.
9. L.A. Chick, L.R. Pederson, G.D. Maupin, J.L. Bates, L.E. Thomas and G.J. Exarhos, *Mater. Lett.* **10** (1990) 6.
10. B.A. Boukamp, *Solid State Ionics* **20** (1986) 31.
11. C.C. Appel, N. Bonanos, A. Horsewell and S. Linderoth, to be published.
12. P. Holtappels, M. Juhl Jørgensen, S. Primdahl, M. Mogensen and C. Bagger, *in* Proceedings of the 3rd European SOFC Forum, 2–5 June, France, edited by P. Stevens (1998), p. 311.
13. G.Ø. Lauvstad, R. Tunold and S. Sunde, *in* Proceedings of the 7th IEA SOFC Workshop: 'Theory and Measurement of Microscale Processes in Solid Oxide Fuel Cells', Norway (1995), p. 41.
14. H. Tsukuda and A. Yamashita, *in* Proceedings of the First European Fuel Cell Forum, Switzerland, edited by U. Bossel (1994), p. 715.
15. L. Bay and T. Jacobsen, *Solid State Ionics* **93** (1997) 201.
16. L. Bay and T. Jacobsen, *in* Proceedings of the 10th IEA SOFC Workshop: 'Materials and Processes', Switzerland (1997), p. 142.
17. G.J. Yurek and H. Schmalzried, *Ber. Bunsenges. Phys. Chem.* **79** (1975) 255.
18. D. Monceau, M. Filal, M. Tebtoub, C. Petot, G. Petot-Ervas, *Solid State Ionics* **73** (1994) 221.
19. J.-O. Hong and H.-I. Yoo, *Solid State Ionics* **113**–**115** (1998) 265.
20. H.-I. Yoo and K.-C. Lee, *J. Electrochem. Soc.* **145** (1998) 4243.
21. C. Bagger, M. Juhl, P.V. Hendriksen, P.H. Larsen, M. Mogensen, J.G. Larsen and S. Pehrson, *in* Proceedings of 2nd European SOFC Forum, Norway, edited by B. Thorstensen (1996), p. 175.
22. C.C. Appel, 'Geological Survey of Denmark and Greenland', Denmark, unpublished result.